Optogenetic silencing strategies differ in their effects on inhibitory synaptic transmission

Joseph V. Raimondo[1], Louise Kay[1], Tommas J. Ellender[1] and Colin J. Akerman[1]

[1]Department of Pharmacology, Oxford University, Oxford, United Kingdom

Supplementary Figures:

Supplementary Figure 1	Shifts in E_{GABAA} resulting from prolonged Cl^- influxes are a general feature of mature GABAergic synaptic transmission.
Supplementary Figure 2	The regulation of E_{GABAA} is similar in neurons from organotypic and acute hippocampal slices.
Supplementary Figure 3	Basic properties of optogenetic silencers.
Supplementary Figure 4	A single compartment model of Cl^- accumulation and extrusion predicts photocurrent induced changes in E_{GABAA}.
Supplementary Figure 5	In vivo virally-driven expression of optogenetic silencers have different effects upon GABAergic transmission in acute slices.
Supplementary Figure 6	GABAergic transmission remains stable in Arch-expressing neurons and their neighbours.
Supplementary Figure 7	Depolarizing shifts in E_{GABAA} are a general consequence of silencing neural activity with a light-activated Cl^- pump.

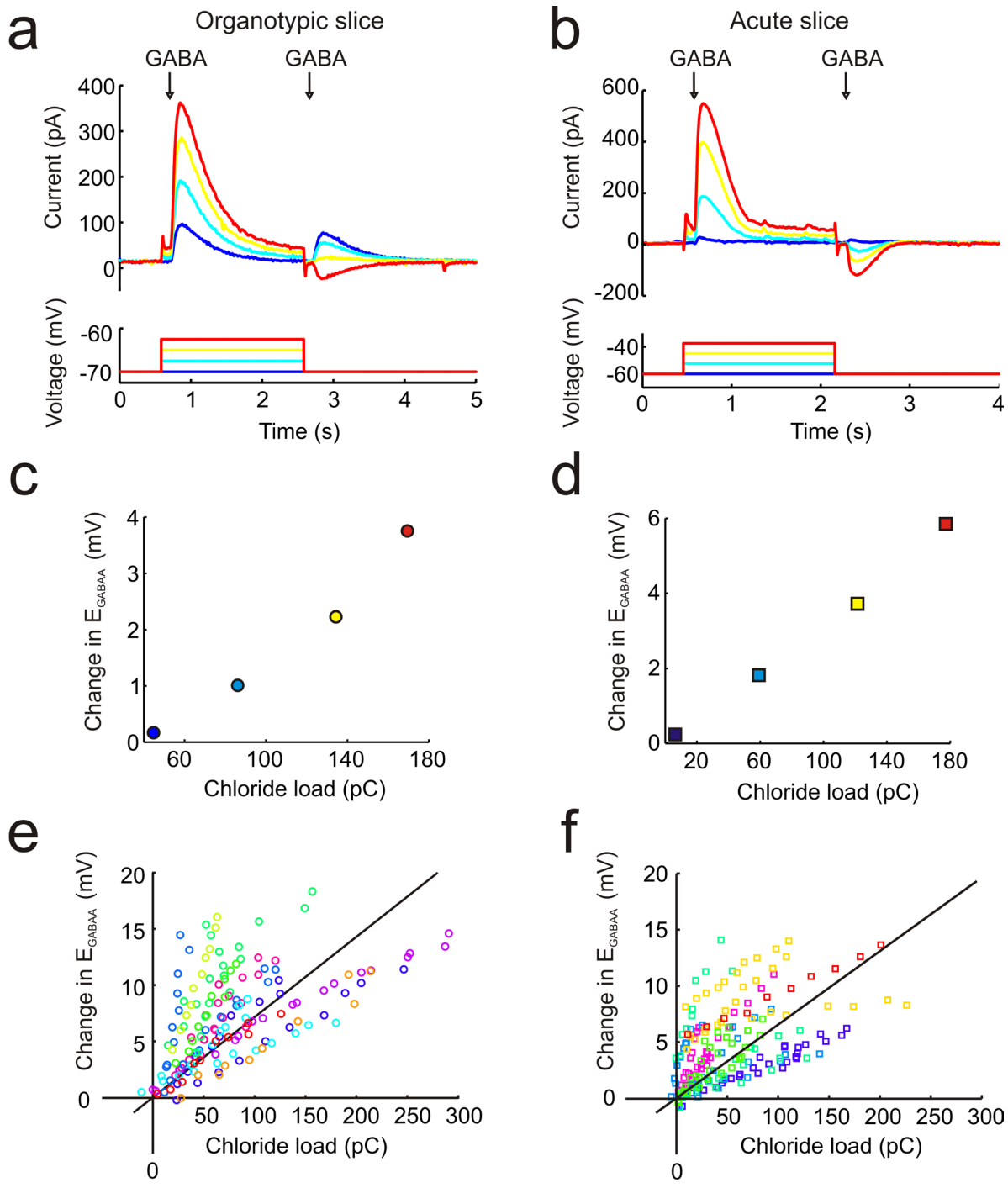

Supplementary Figure 1. Shifts in E_{GABAA} resulting from prolonged Cl^- influxes are a general feature of mature GABAergic synaptic transmission. (**a**) Gramicidin perforated patch voltage clamp recording from a CA3 pyramidal neuron in an organotypic hippocampal slice (**Supplementary Methods**). Different sized Cl^- loads were elicited by stepping the membrane voltage to different potentials for 2 s and activating $GABA_AR$s simultaneously with a GABA puff (100 μM; 100 ms after the start of the voltage step). Larger depolarizing voltage steps resulted in stronger driving forces on the $GABA_AR$ and therefore larger Cl^- loads. 100ms after the end of the voltage step (and therefore 2s after the first GABA puff) a second GABA puff was

delivered to estimate whether E_{GABAA} had changed as a result of the Cl^- load. Note that larger Cl^- loads can switch the direction of the $GABA_AR$ current from outward to inward. (**b**) Similar data for a pyramidal neuron recorded from an acute hippocampal slice (aged 4 weeks). Note again that larger Cl^- loads switch the direction of the $GABA_AR$ current from outward to inward. (**c**) and (**d**) show the change in E_{GABAA} caused by the different Cl^- loads in the recordings from the cells in 'a' and 'b', respectively (colour-coded by trace). (**e**) Summary data from organotypic slices (n = 10 cells) showing the strong positive correlation between the size of the $GABA_AR$-mediated Cl^- load and the resulting change in E_{GABAA} ($r = 0.54$, $P < 1x10^{-12}$, Pearson Correlation). Data from individual neurons are coded by colour. (**f**) Summary data from acute hippocampal slices (n = 7 cells) showing a similar positive correlation between the size of the $GABA_AR$-mediated Cl^- load and the resulting change in E_{GABAA} ($r = 0.50$, $P < 1x10^{-12}$, Pearson Correlation). Data from individual neurons are coded by colour. As E_{GABAA} values after a Cl^- load reflect the rate of recovery via endogenous extrusion mechanisms, these data show that acute and organotypic slices have a similar capacity for Cl^- transport (Brumback, A.C., Staley, K.J. 2008 *J Neurosci* 28, 1301-12; Jin, X., Huguenard, J.R., Prince, D.A. 2005 *J Neurophysiol.* 93, 2117-26).

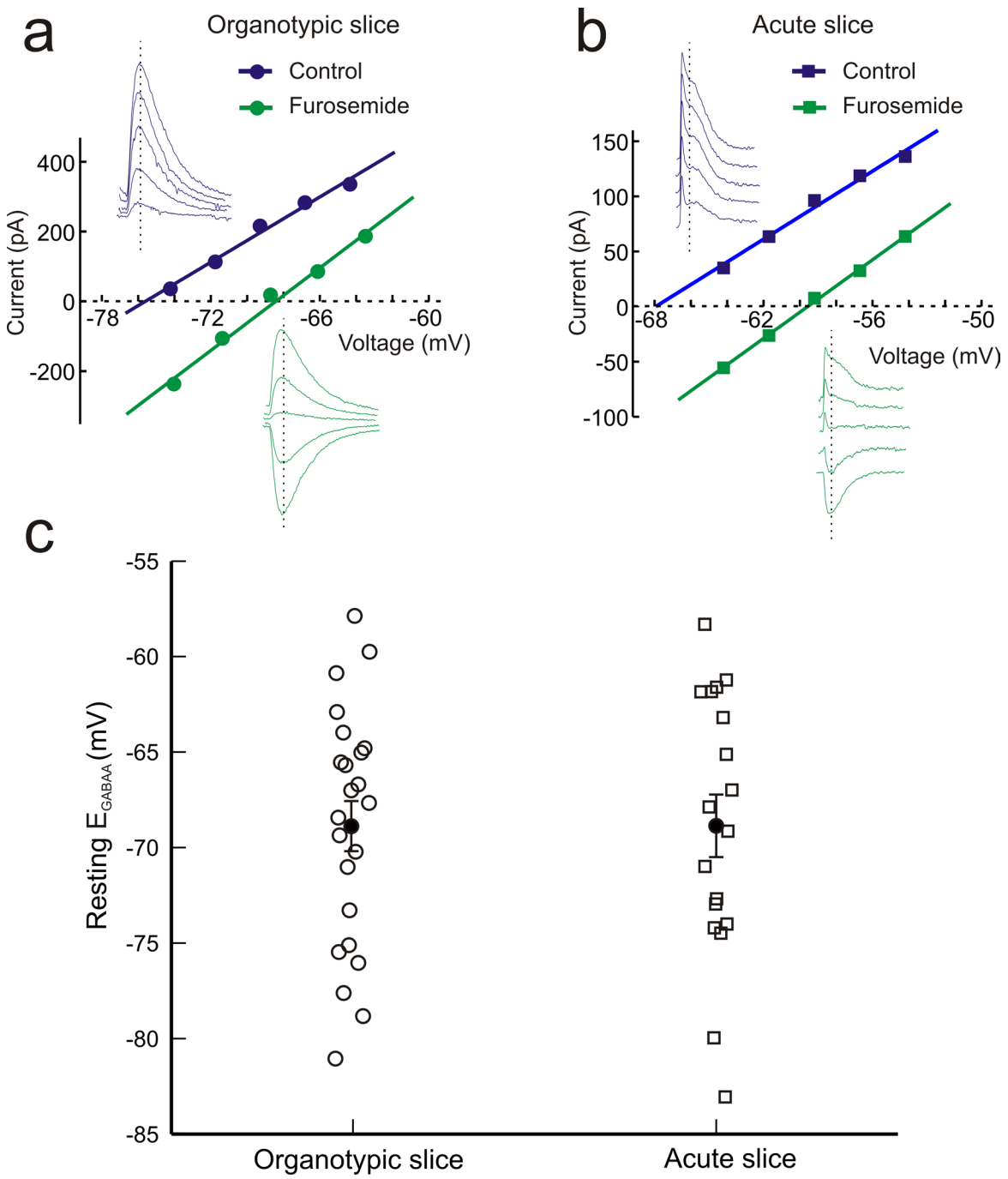

Supplementary Figure 2. The regulation of E_{GABAA} is similar in neurons from organotypic and acute hippocampal slices. (**a**) Gramicidin perforated patch voltage clamp recording from a pyramidal neuron in an organotypic hippocampal slice. E_{GABAA} shifted from -75.6 to -68.2 mV after the application of furosemide (200 μM) - an inhibitor of cation-chloride cotransporter proteins. (**b**) Data for a pyramidal neuron recorded from an acute hippocampal slice where E_{GABAA} shifted from -67.9 to -59.1 mV after addition of furosemide (aged 4 weeks) showing a similar contribution of cation-chloride cotransporter proteins to E_{GABAA}. (**c**) Summary data for organotypic (n = 23 cells) and acute (n = 18 cells) hippocampal slices showing a comparable mean and range for resting E_{GABAA} values. The two groups were statistically indistinguishable (P = 0.99, Student's t-test).

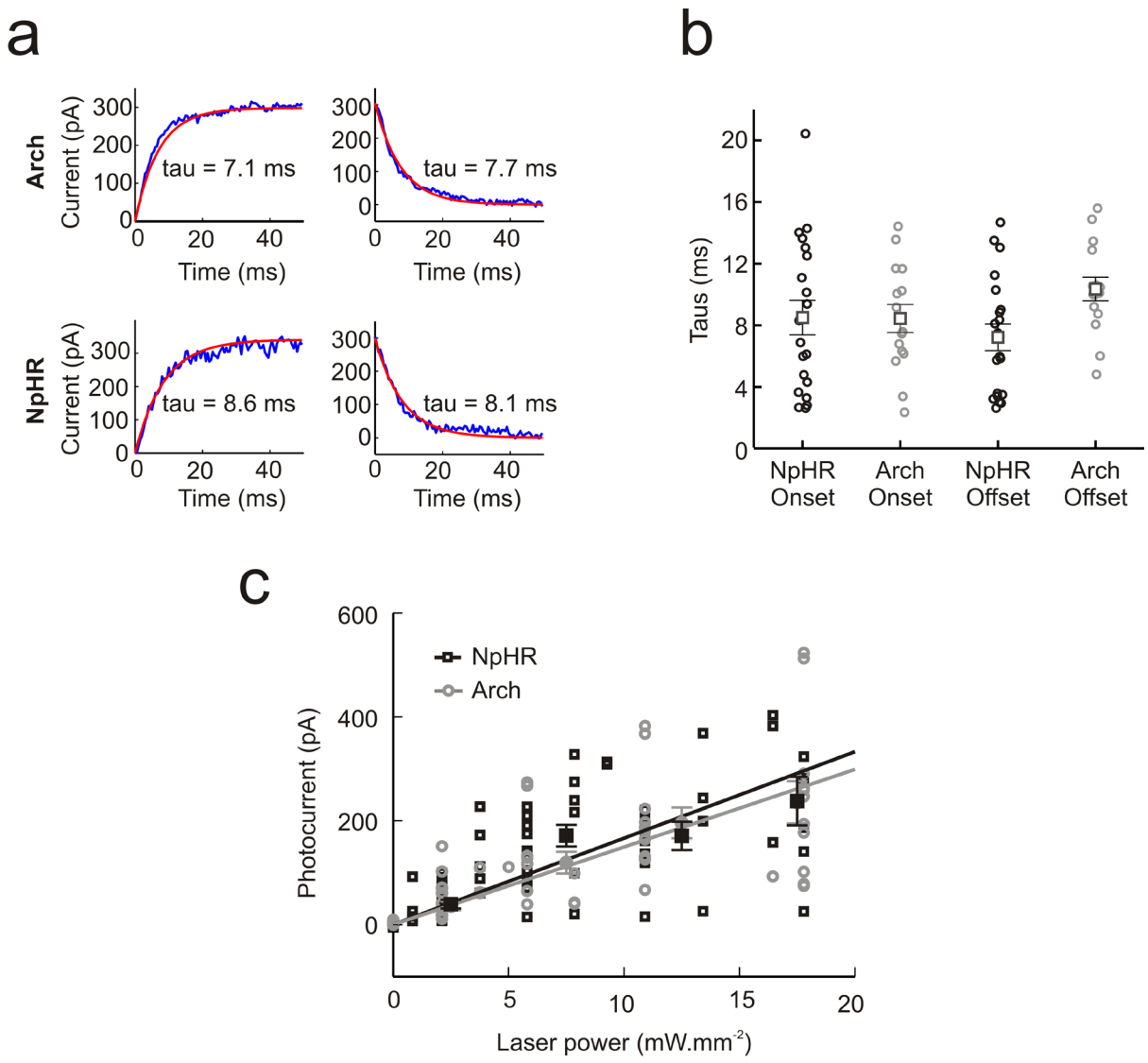

Supplementary Figure 3. Basic properties of optogenetic silencers. (**a**) Gramicidin perforated patch voltage clamp recordings from a neuron expressing Arch (top) and a separate neuron expressing eNpHR3.0 (bottom) immediately following laser onset (left) and immediately following laser offset (right). Activation and deactivation kinetics could be fitted with a single exponential function (red) and the time constants were fast. (**b**) Population data shows that the time constant for both Arch and NpHR onset and offset are comparable and fast (<10 ms, on average). (**c**) Mean photocurrent amplitude plotted as a function of laser power for Arch- and eNpHR3.0-expressing neurons. This relationship was statistically indistinguishable for the two optical silencers, suggesting that a particular laser power would generate photocurrents of comparable amplitude under our recording conditions (P = 0.7074, Analysis of Covariance).

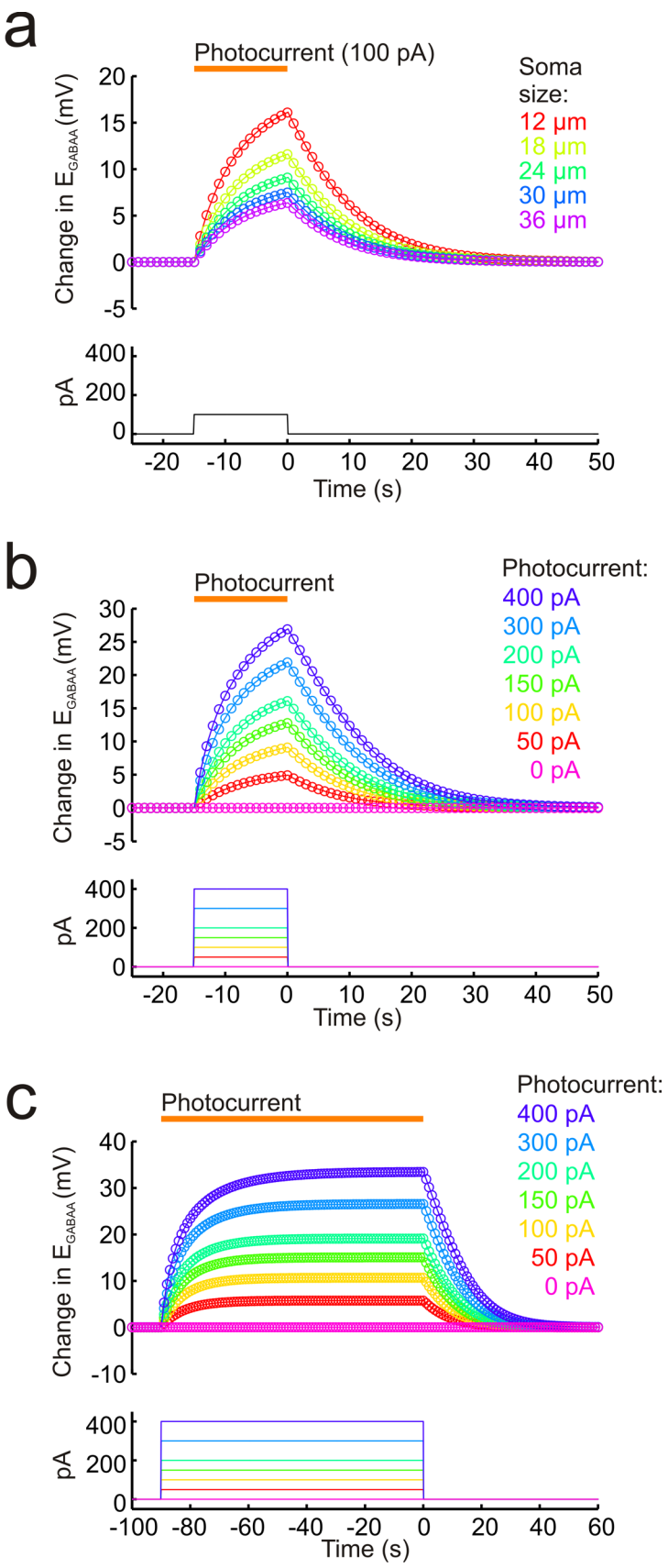

Supplementary Figure 4: A single compartment model of Cl^- accumulation and extrusion predicts photocurrent induced changes in E_{GABAA}. Details of the model are provided below. (**a**) A 100 pA Cl^- photocurrent was applied to somata of varying

volumes for a period of 15 s. Soma volume was modeled as a prolate spheroid, in which the soma width was held constant at 12 µm whilst the soma length was varied between 12 and 36 µm. For all soma sizes, E_{GABAA} can be seen to increase steadily over the course of the modeled photocurrent. Following the end of the photocurrent, E_{GABAA} was at more positive values and then recovered to baseline over the course of 15 to 30 s. A soma length of 24 µm resulted in an E_{GABAA} shift of 9.1 mV by the end of the photocurrent, which was equivalent to the size of E_{GABAA} shift measured experimentally for a photocurrent of 100 pA (see **Fig. 2d**). (**b**) Cl^- photocurrents with a duration of 15 s, and amplitudes between 0 and 400 pA, were applied to a soma with a length of 24 µm (as in 'a'). The size of the change in E_{GABAA} was proportional to the magnitude of the photocurrent induced. Also note that the time for E_{GABAA} to recover to baseline values (between 20 and 40 s) was related to the size of the photocurrent. (**c**) Modeling photocurrents of 90 s in duration demonstrated that depolarizing shifts in E_{GABAA} stabilize after approximately 40 s, at values that are dependent upon the size of the induced photocurrent.

The details of the model were as follows: E_{GABAA} was based on a receptor permeability for Cl^- that is four times that of HCO_3^- (Kaila, K. 1994 *Prog Neurobiol.* 42, 489-537). Intracellular and extracellular HCO_3^- concentrations were held constant at 10 mM and 25 mM, respectively (Lambert, N., Grover, L. 1995 *Science* 269, 928–9). A stable extracellular Cl^- concentration of 135 mM was used and intracellular Cl^- was able to vary dynamically. E_{GABAA} was calculated at each time-step using the Goldman-Hodgkin-Katz equation. The somatic compartment was modelled as a prolate spheroid with volume related to the somatic width and somatic length. To simulate cells of differing volume, somatic length was varied between 12 and 36 µm, whilst somatic width was held constant at 12 µm. These values were based upon measurements from our recorded cells and resulted in neuronal cell volumes of between 0.9 and 2.7 pL, which corresponds to the range of somatic volumes reported for rat hippocampal neurons (Ambros-Ingerson, J., Holmes, W.R. 2005 *Hippocampus* 15, 302-15).

Consistent with previous work, we modelled the rate of Cl^- transport by KCC2 in analogy to Ohm's law where current flow is equal to the driving force multiplied by the conductance (Brumback, A.C., Staley, K.J. 2008 *J Neurosci* 28, 1301-12). The combined K^+ and Cl^- electrochemical gradient creates the driving force whilst the transport capacity represents the conductance. The driving force or change in free energy (ΔG) is a result of the transmembrane concentration gradients of the transported ions:

$$\Delta G = -\frac{RT}{F}\ln\left(\frac{[Cl^-]_o[K^+]_o}{[Cl^-]_i[K^+]_i}\right)$$

In order to create a dimensionless term, free energy (ΔG) was normalised to ΔG_{max}. Using a method similar to that employed by Brumback and Staley (2008), ΔG_{max} was calculated by using the maximum $[Cl^-]_i$ that was measured following a Cl^- load in our recordings (56 mM). The transport capacity of KCC2 (V_{mm}) was modelled using Michaelis-Menten kinetics for enzymatic activity (Staley, K.J., Proctor, W.R. 1999 *J Physiol*. 519, 693-712; Russell, J.M. 2000 *Physiol Rev.* 80, 211-76).

$$V_{mm} = \frac{V_{max}\,[Cl^-]_i}{K_d + [Cl^-]_i}$$

Where $[Cl^-]_i$ is the substrate concentration for outward transport of Cl^-, V_{max} is the maximum velocity of Cl^- transport, and K_d is the $[Cl^-]_i$ where transport is half maximal. The values for V_{max} and K_d (5 mM/s and 15 mM) used in our model were taken directly from Staley and Proctor (1999).

The velocity of KCC2-mediated Cl^- transport (in mM/s) is therefore calculated by multiplying the normalized driving force $\Delta G/\Delta G_{max}$ by the conductance term V_{mm} as in Brumback and Staley (2008):

$$V_{KCC2} = \frac{\Delta G}{\Delta G_{max}} \times V_{mm}$$

A tonic Cl^- current was calculated that would maintain resting $[Cl^-]_i$ at 7 mM in order to achieve a baseline E_{GABAA} of -70 mV, consistent with our recordings (see Supplementary Fig. 2). A Cl^- 'photocurrent' of varying amplitude and duration could then be applied and the resulting changes in $[Cl^-]_i$ and hence E_{GABAA} tracked over time using the following equation:

$$[Cl^-]_{i,t+1} = [Cl^-]_{i,t} + \left[\frac{(I_{tonic} + I_{photocurrent})}{F} - V_{KCC2}.Vol\right]\frac{\Delta t}{Vol}$$

It should be noted that NpHR photocurrents can be maintained in the face of intracellular chloride accumulation because of the pump's extremely negative reversal potential (approximately -400 mV; Seki, A., Miyauchi, S., Hayashi, S., Kikukawa, T., Kubo, M., Demura, M., Ganapathy, V., Kamo, N. 2007 *Biophys J.* 92, 2559-69).

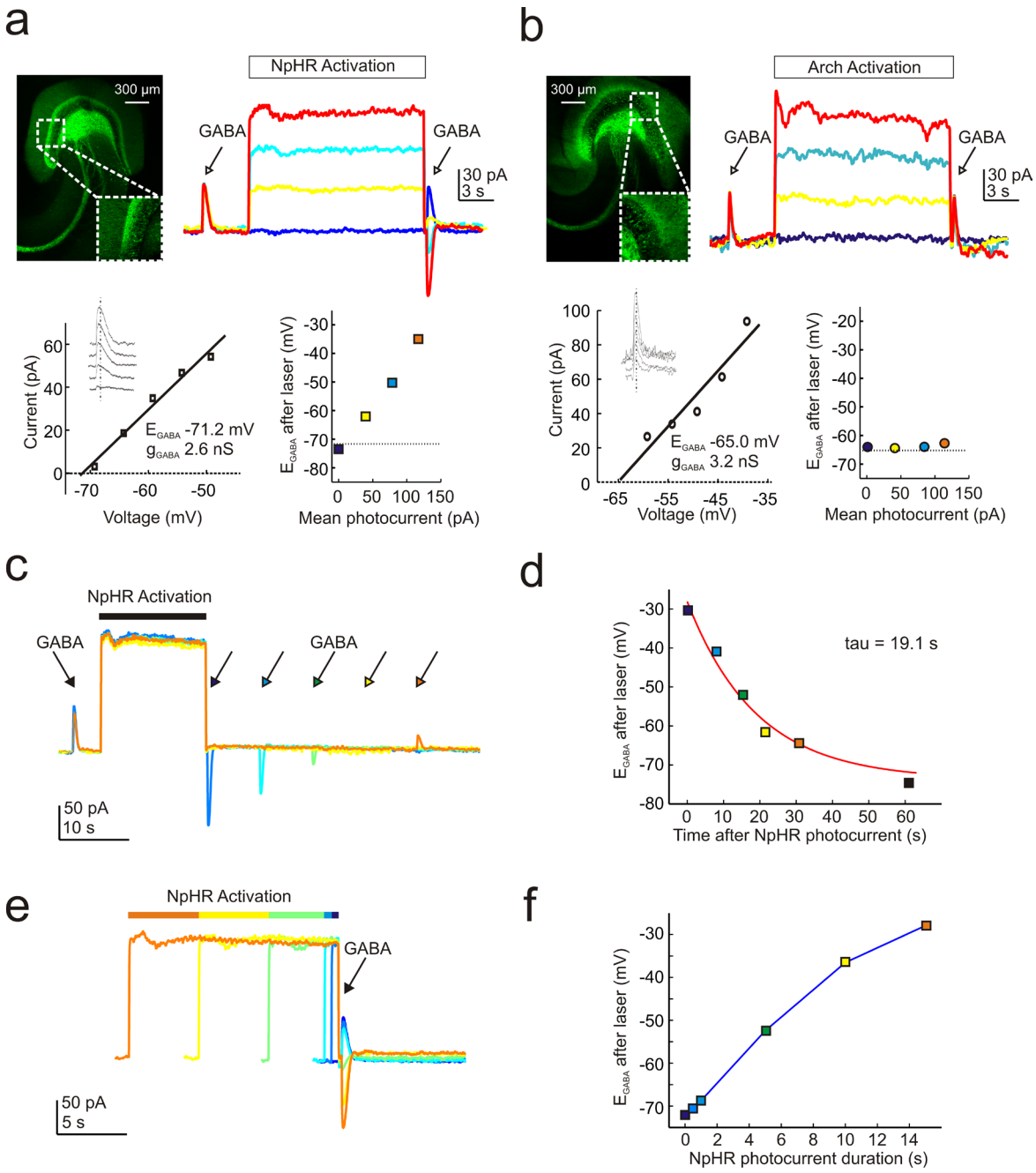

Supplementary Figure 5. In vivo virally-driven expression of optogenetic silencers have different effects upon GABAergic transmission in acute slices. (**a**) Top left, a 2-photon image showing widespread expression of eNpHR3.0-EYFP in the dentate gyrus. Top right, gramicidin perforated patch voltage clamp recording from an eNpHR3.0-expressing neuron in this slice. $GABA_AR$ currents were measured before and after NpHR-activation for 15 s, at four different laser intensities. Bottom left, $GABA_AR$ IV plots were used to calculate the resting E_{GABAA} and $GABA_AR$ conductance (g_{GABAA}), which were then used to estimate E_{GABAA} for individual GABA puffs delivered after different mean photocurrents (bottom right). (**b**) Top left, a 2-photon image showing widespread expression of Arch-GFP in the dentate gyrus. Top right, recordings from an Arch-expressing neuron in this slice. Bottom left and right, all conventions as in 'a'. Note the stable $GABA_AR$ current following different levels of Arch-activation. (**c**) Traces from a representative NpHR-expressing neuron

showing $GABA_AR$ currents recorded at different times after the photocurrent, on different trials. (**d**) E_{GABAA} versus time after photocurrent is plotted for this cell and the recovery is well fitted by a single-exponential function. (**e**) Traces from a representative NpHR-expressing neuron showing $GABA_AR$ currents recorded after photocurrents of different durations. (**f**) E_{GABAA} measured after the laser in this cell, plotted as a function of photocurrent duration.

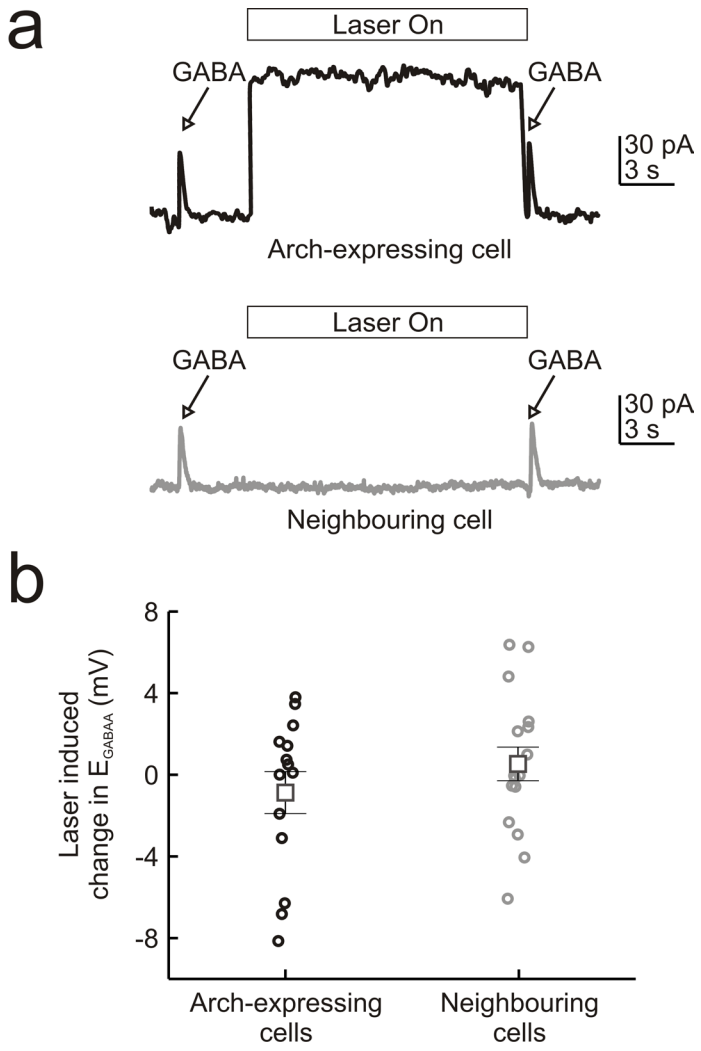

Supplementary Figure 6. GABAergic transmission remains stable in Arch-expressing neurons and their neighbours. Changes in H^+ concentration could theoretically affect E_{GABAA} by altering the amount of bicarbonate that is free to flow through the $GABA_AR$ (Kaila, K. 1994 *Prog Neurobiol.* 42, 489-537) or by changing the driving force on bicarbonate-chloride exchange proteins (Sterling, D. 1999 *Biochem. J.* 229, 221–229; Svichar, N., Waheed, A., Sly, W.S., Hennings, J.C., Hübner, C.A., Chesler, M. 2009 *J Neurosci*. 29, 3252-3258). However, we found no evidence that Arch photocurrents affect E_{GABAA} in Arch-expressing neurons or in neighbouring cells. (**a**) Gramicidin perforated patch voltage clamp recording from a neuron expressing Arch (top) and a neighbouring neuron (bottom), from tissue containing widespread expression of Arch (see **Supplementary Figure 4).** $GABA_AR$ currents were measured before and after presentation of the laser ('laser on'). (**b**) Summary data confirms that in tissue with widespread expression of Arch, neither expressing (-0.87 ± 1.03 mV, P = 0.4121, t test) nor non-expressing neighbouring neurons (0.44 ± 0.82 mV, P = 0.60, t test) show changes in E_{GABAA} following laser activation.

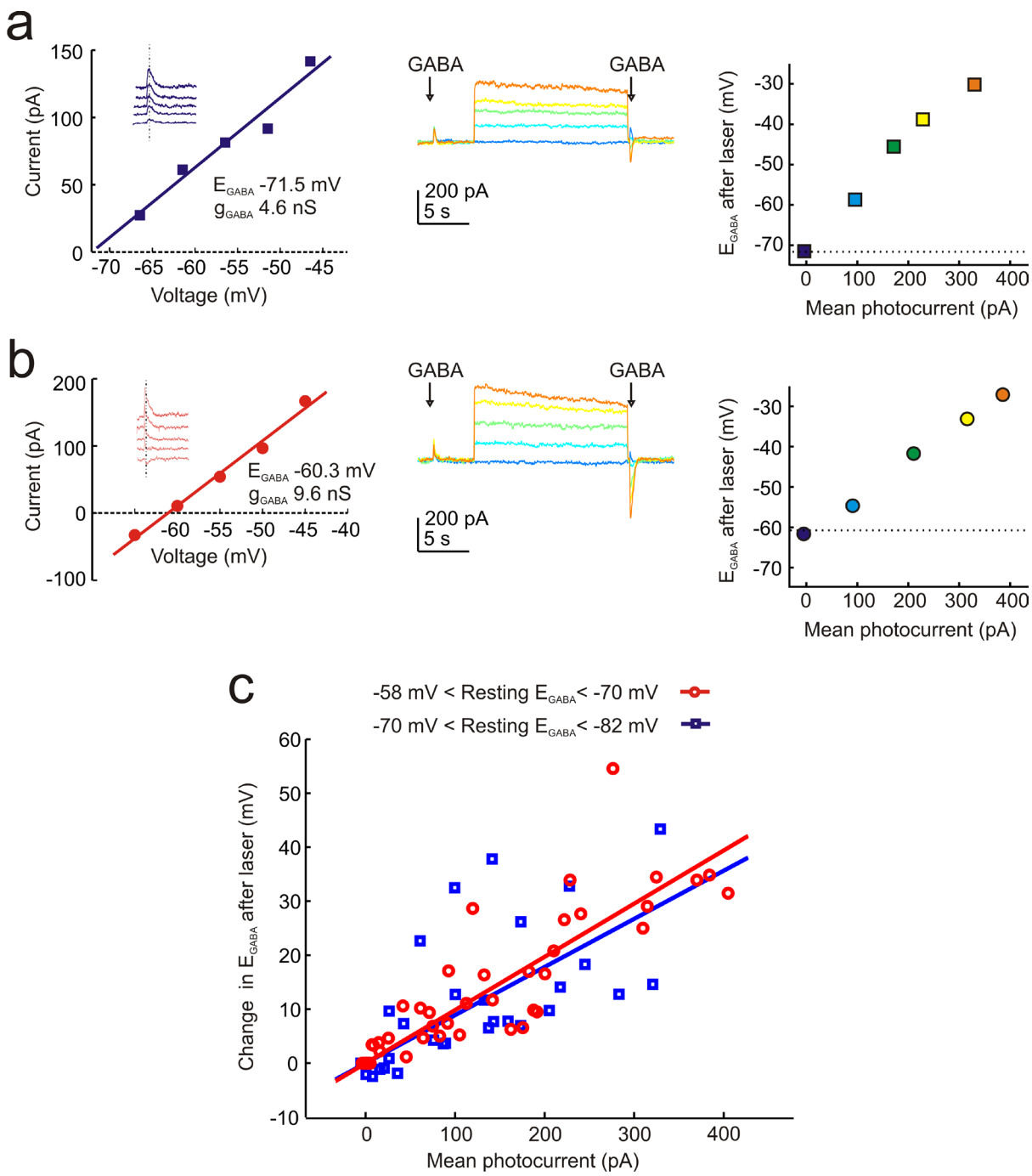

Supplementary Figure 7. Depolarizing shifts in E_{GABAA} are a general consequence of silencing neural activity with a light-activated Cl^- pump. When neurons were divided into those with relatively more, or less, hyperpolarized resting E_{GABAA} values, both groups showed significant depolarizing shifts in E_{GABAA}. (**a**) Gramicidin perforated patch recording from an eNpHR3.0-EYFP expressing neuron, which had a relatively hyperpolarized resting E_{GABAA} (-71.5 mV). A $GABA_AR$ IV plot (left) was used to calculate the resting E_{GABAA} and $GABA_AR$ conductance (g_{GABAA}). These were then used to estimate E_{GABAA} for individual GABA puffs delivered after different mean photocurrents (middle and right, colour-coded by trace). (**b**) Gramicidin perforated patch voltage clamp recording from an eNpHR3.0-EYFP expressing neuron, which had a relatively depolarized resting E_{GABAA} (-60.3 mV). (**c**) Summary of the change in

E_{GABAA} associated with different NpHR photocurrents, with the data divided into neurons with more hyperpolarized resting E_{GABAA} values (-70 mV to -82 mV; *n* = 6 cells; blue symbols) and less hyperpolarized resting E_{GABAA} values (-58 mV to -70 mV; *n* = 5 cells; red symbols). The two populations displayed similar shifts in E_{GABAA} and similar positive correlations between photocurrent size and the change in E_{GABAA}. For the more hyperpolarized group the slope of the linear fit was 8.9 mV per 100 pA photocurrent *(r* = 0.68, *P* < $1x10^{-5}$, Pearson Correlation) and for the less hyperpolarized group the slope of the linear fit was 9.8 mV per 100 pA photocurrent (r = 0.86, *P* < $1x10^{-5}$, Pearson Correlation).